Proceedings of HTSC 2005:
Heat Transfer Summer Conference
San Francisco, CA, July 17-22, 2005

HT2005-72291

HEAT TRANSFER IN ULTRAFAST LASER TISSUE WELDING

Kyunghan Kim, Zhixiong Guo*
Department of Mechanical and Aerospace Engineering
Rutgers, The State University of New Jersey
Piscataway, NJ 08854

Sunil Kumar
Department of Mechanical Engineering
Polytechnic University
Brooklyn, NY 11201

ABSTRACT

The objective of this research is to develop an appropriate model for simulating the transient heat transfer processes in tissue welding subject to irradiation of ultrashort laser pulses. The ultrafast laser tissue welding process is modeled in three steps. First, there is an immediate local temperature response due to radiation absorption during an ultrashort time period. The transient discrete ordinate method is employed to simulate the ultrashort laser pulse transport in tissue. The temporal radiation field is obtained and the lumped method is used for predicting the local temperature response. After a stable local temperature profile is achieved, the second step starts, in which the hyperbolic heat conduction model is adopted to describe the heat transfer. The thermal wave behavior is observed. It is found that the hyperbolic wave model predicts a higher temperature rise than the classical diffusion model. After about five thermal relaxation times the thermal wave behavior is substantially weakened and the heat diffusion predominates. The heat diffusion equation can accurately describe the heat transfer thereafter.

INTRODUCTION

Since the first report on laser radiation [1], many practical and potential applications have been investigated. Among them, medical laser surgery – a special laser material processing – certainly belongs to the most significant advances of the past several decades. Laser welding of tissue is a surgical technique for bonding of tissues by using a laser beam to activate photothermal bonds and/or photochemical bonds. This method is potentially more advantageous than the conventional suturing technique because it is a non-contact method, which does not introduce foreign materials, and it is capable of forming an immediate watertight seal. For over 30 years, laser tissue welding has been extensively studied [2-4] as an alternative tool for tissue closure.

Laser tissue welding can be augmented with the use of solders [5]. The solders can include chromophores that are used to control the laser penetration such that it is concentrated at the fusion site. Since extrinsic chromophores are not limited to the absorption characteristic of native tissue or body fluids, the solders may be tailored to selectively absorb energy that passes through normal tissue. The solders can also include other biochemical constituents to improve the weld strength and/or weld leakage characteristics. Typical additives include native collagen, gelatinous collagen, fibrin, elastin and albumin.

Suitable lasers deliver wavelengths that are highly absorbed either by water (a major component in tissues), or the tissue's natural chromophores, or solders (in the case of laser soldering). For example, argon lasers (488 and 514 nm) and KTP lasers (532 nm) were used with hemoglobin [6]; Nd:YAG (1.064 and 1.320 μm) and CO_2 (10.6 μm) lasers were used with water [7]. The peak absorption wavelengths of two commonly used chromophores - indocyanine green (ICG) and methylene blue (MB) - are 805 nm and 665 nm in protein solder [8], respectively.

Independent of the choice of chromophores, more energy is generally absorbed near the upper portion of the solder, closer to the laser spot. A temperature gradient is then established over the depth of the solder. Depending on the temperature gradient and the laser exposure, the upper portion of the solder can become over-coagulated while the most critical region, such as the solder/tissue interface, does not get fully coagulated. Such under-coagulated soldering has been shown to create unstable bonds with tissue [5]. Hence, clinical use of laser welding and soldering has been limited [2] because of unreliable fusion strength, possibly excessive thermal

* Corresponding author, guo@jove.rutgers.edu

damage of tissue, non-uniformity in heating, etc. Further research both numerically and experimentally is required.

Prediction of thermal response is a critical issue in laser tissue welding and soldering in order to choose optimal laser parameters including wavelength, pulse duration and repetition rate, beam size and shape, output power, and so on. In order to achieve optimum welding strength, a proper temperature at the welding region was reported at 62.2 ± 2°C [9]. Pulsed lasers were applied to reduce the collateral thermal damage [10, 11]. With the rapid advance of laser technology, the current state-of-the-art ultrafast lasers can reach to ultrashort time duration of a few femtoseconds. Of course, femtosecond lasers are generally considered for use in laser ablation due to their extremely high flux. But picosecond lasers with moderate output power may be considered for tissue welding and/or soldering. To this end, it is needed to simulate heat transfer in ultrafast laser tissue welding and/or soldering which can be modeled as a coupled radiative-conductive heat transfer problem.

First the knowledge of radiation heat transfer in tissues must be understood. This involves the solution of time-dependent equation of radiation transfer for predicting ultrafast laser radiation absorption inside a tissue. In recent years, the research on ultrafast laser transport in turbid media has attracted increasing attention [12]. The present authors have extensively studied this topic in a series of their publications [13-16] under various conditions. Most recently Kim and Guo [17] numerically investigated radiation heat transfer in ultrafast laser tissue welding and soldering using high-order of accuracy discrete-ordinate method (DOM).

Second the temperature field is modeled as a heat conduction problem. For irradiation times less than 10 sec, the influence of blood perfusion plays a minor role and is negligible [18]. Fourier heat conduction equation (parabolic type) implies an infinite speed of thermal propagation and is traditionally used for describing heat diffusion. For a physical process occurring in very short time interval than that required for attaining thermal equilibrium, however, it has been noticed that heat wave theory must be adopted [19-21]. The thermal wave postulate leads to hyperbolic heat conduction equations and suggests a finite speed of thermal propagation. Mitra et al. [22] and Tzou [23] provided some experimental evidences of hyperbolic heat conduction. Thermodynamic validity of the hyperbolic equations and the range of parameters where non-Fourier considerations are significant have also been examined [24, 25]. Glass et al. [26] approached the hyperbolic conduction problems numerically using MacCormack's scheme. Some other numerical methods [27-30] have also been recently developed.

Vedavarz et al. [25] have analyzed the relaxation time of thermal wave for various materials. They found that the relaxation time of biological tissues was in the range of 1-100 sec at room temperature, which are several orders of magnitude larger than that of metallic and semiconductor materials. Kaminski [20] estimated the thermal relaxation time between 20 and 30 sec for meat products. Mitra et al. [22] measured a 16 sec thermal relaxation time for processed meat. Such larger relaxation times in biological tissues make the hyperbolic heat conduction specifically significant in the thermal modeling of laser-tissue interactions.

The objective of this work is to analyze the thermal response in tissues subjected to irradiation of ultrashort laser pulses with potential applications to ultrafast laser tissue welding and soldering and other medical applications of lasers in which thermal effects are significant. In the present study, the ultrafast radiation heat transfer in tissues is governed by the time-dependent equation of radiation transfer (ERT) in which the radiation wave is propagated with the speed of light. The transient ERT is solved using the transient DOM method. The hyperbolic heat conduction equations are solved using the finite difference method based on MacCormark's scheme. The speed of thermal wave is several orders of magnitude smaller than that of light. Thus, the coupling of radiative-conductive heat transfer involves two different time scales. In order to examine the non-Fourier effects, the transient thermal responses obtained from hyperbolic heat conduction modeling are compared with those obtained from the classical parabolic heat diffusion equation.

MATHEMATICAL MODELS

Governing Equations

The speed of thermal wave c_t is defined as

$$c_t = \sqrt{\alpha/\tau} \quad , \tag{1}$$

where α is the thermal diffusivity and τ is the thermal relaxation time. The reported thermal diffusivity of tissues is in the range of 0.1 – 0.2 mm^2/s [31,32]. Suppose α = 0.15 mm^2/s and τ = 15 s, then c_t = 0.1 mm/s.

Radiation is transported in the speed of light, i.e. c = 0.2 mm/ps in tissue. It is 12 orders of magnitude faster than the speed of thermal wave. Thus, during the time scale of ultrafast radiation transport (less than 1 ns) the transport of thermal wave is negligible. The heat transfer in ultrafast laser-tissue interaction is a multi-scale and multi-physics problem.

Consider a collimated laser pulse incidence upon a 2-D biological tissue shown in Fig. 1. The local temperature response of the tissue to an ultrashort laser pulse can be simply expressed as

$$\rho C_p \frac{\partial T(x,y,t)}{\partial t} = \nabla \cdot q_{rad}(x,y,t) , \tag{2}$$

where $\nabla \cdot q_{rad}(x,y,t)$ is the divergence of radiative heat flux due to radiation absorption that is calculated by

$$\nabla \cdot q_{rad}(x,y,t) = \sigma_a (4\pi I_b - G) , \tag{3}$$

where σ_a is the absorption coefficient of the tissue and I_b is the black body emissive power which is negligible because the tissue can be treated as a cold medium as compared to the large flux of laser beam. The incident radiation, G, is a direction-integrated radiation intensity and can be obtained by the summation of angle-discretized radiation intensity.

To calculate the radiative intensity I^l in a discrete ordinate, time-dependent ERT in discrete-ordinate format is introduced:

$$\frac{1}{c}\frac{\partial I^l}{\partial t}+\xi^l\frac{\partial I^l}{\partial x}+\eta^l\frac{\partial I^l}{\partial y}+\sigma_e I^l=\sigma_e S^l, l=1,2,3,...,n \quad (4)$$

where ξ^l and η^l are the directional cosine in a discrete ordinate direction, σ_e is the extinction coefficient that is the sum of the absorption and scattering coefficients, and S^l is the radiative source term from the laser radiation.

After the ultrashort pulse effect is diminished in a very short time period, the temperature response reaches to a pseudo steady state; and then thermal wave transport starts. To predict the transient temperature field during thermal wave transport, the hyperbolic heat conduction equations are introduced [19-21]:

$$\tau\frac{\partial q_{cond,x}(x,t)}{\partial t}+q_{cond,x}(x,t)=-k\frac{\partial T(x,y,t)}{\partial x}, \quad (5\text{-}1)$$

$$\tau\frac{\partial q_{cond,y}(y,t)}{\partial t}+q_{cond,y}(y,t)=-k\frac{\partial T(x,y,t)}{\partial y}. \quad (5\text{-}2)$$

where k is the thermal conductivity, T and q represent temperature and heat flux, respectively.

The energy equation is expressed as

$$\rho C_p\frac{\partial T(x,y,t)}{\partial t}=-\left(\frac{\partial q_{cond,x}(x,t)}{\partial x}+\frac{\partial q_{cond,y}(y,t)}{\partial y}\right). \quad (6)$$

Here ρ is the density and C_p the specific heat.

For the sake of analysis, the hyperbolic conduction equations and energy equation are converted to non-dimensional forms as follows:

$$\frac{\partial Q_\chi}{\partial\xi}+\frac{\partial\theta}{\partial\chi}+10Q_\chi=0, \quad (7\text{-}1)$$

$$\frac{\partial Q_\eta}{\partial\xi}+\frac{\partial\theta}{\partial\eta}+10Q_\eta=0, \quad (7\text{-}2)$$

$$\frac{\partial\theta}{\partial\xi}+\frac{\partial Q_\chi}{\partial\chi}+\frac{\partial Q_\eta}{\partial\eta}=0, \quad (7\text{-}3)$$

where non-dimensional variables are defined by

$$Q_\chi=\frac{q_{cond,x}\sqrt{\alpha\tau}}{k(T_{ref}-T_i)},\ Q_\eta=\frac{q_{cond,y}\sqrt{\alpha\tau}}{k(T_{ref}-T_i)},\ \theta=\frac{T-T_i}{T_{ref}-T_i},$$

$$\chi=\frac{x}{10\sqrt{\alpha\tau}},\ \eta=\frac{y}{10\sqrt{\alpha\tau}},\ \xi=\frac{t}{10\tau}. \quad (8)$$

In which, T_i and T_{ref} are the cold tissue and reference temperatures, respectively.

Boundary Conditions

For radiation heat transfer, reflection and refraction governed by Snell's law and Fresnel equation, respectively, are considered at the tissue/are interface. At the rest boundaries, diffuse reflections are considered. For details, please refer to our recent publications [16, 17].

The incident laser sheet has a Gaussian profile both temporally and spatially and can be expressed by

$$I_c(x,y,t)=I_{c0}\exp\left\{-4\ln 2\times[(t-x/c)/t_p-2]^2\right\}\times\exp[-(y-W/2)^2/\nu^2]\times\exp(-\sigma_e x) \quad (9)$$

in which I_{c0} is the peak amplitude of the intensity which is set as 0.06 in the present calculations, t_p is the pulse width, and ν is the spatial variance factor. The Gaussian spatial ratio ν/D is chosen as 1.0, where D is the width of the laser sheet. The reference temperature is calculated from the incident laser pulse by

$$T_{ref}=T_i+\frac{\int_0^{4t_p}\sigma_a I_c(x=0,y=W/2,t)dt}{\rho C_p}. \quad (10)$$

For hyperbolic heat conduction, the boundary conductions are specified below.

$$\theta(\chi,\eta,\xi)=0, \text{ for } \eta=0 \text{ or } \eta=\eta_{\max}=W/(10\sqrt{\alpha\tau}) \quad (11\text{-}1)$$

$$\theta(\chi,\eta,\xi)=0, \text{ for } \chi=\chi_{\max}=L/(10\sqrt{\alpha\tau}) \quad (11\text{-}2)$$

$$Q_x=h^*(\theta-\theta_\infty), \text{ for } \chi=0 \quad (11\text{-}3)$$

where θ_∞ is the non-dimensional ambient temperature and $h^*=\sqrt{\alpha\tau}h/k$. h is the heat transfer coefficient.

The following lists several assumptions we adopted when set up the present model:

(1) The lumped method is used for predicting local temperature response during the ultrashort pulse period. Since the effective laser exposure time for each pulse is less than 1 ns, while the thermal speed in tissue is about 10^{-10} mm/ns, the thermal propagation and diffusion for the local temperature response is negligible.

(2) In order to heat the tissue to target temperature, pulse trains in a short time period are needed. Here we only assume one pulse.

(3) Thermal radiation emission at the tissue/air interface is negligible because the surface temperature is low such that the blackbody intensity is much smaller than the incident laser intensity.

(4) The tissue optical and thermal properties are thermally stable during the tissue welding process.

(5) Thermal evaporation during the welding process is not considered.

(6) The phase change (from solid to soft) of tissue in the welding region is not taken into account.

Numerical Schemes

To solve the time-dependent ERT, the transient DOM is employed. The tissue geometry is divided by a uniform grid system of 200×200. The solid angle is divided by a quadrature set of $M=N(N+2)$ discrete ordinates for S_N method. In the present study, we use the S_{10} scheme. The time step selected is 0.2 ps. Details of the numerical schemes have been described in our recent publications [13-17]; thus, they are not repeated here.

To solve the hyperbolic heat conduction equations, MacCormack's predictor-corrector scheme is adopted. The hyperbolic equations include the discontinuities in front of thermal wave. MacCormack's predictor-corrector scheme has been known to deal with wave propagation very well in a 1-D hyperbolic heat conduction problem [26]. Thus, it is extended to the 2-D problem in the present study. The discretized forms of these equations are as follows:

Predictor:

$$\tilde{Q}_{x\,i,j}^{n+1} = (1-10\Delta\xi)\, Q_{x\,i,j}^{n} - \frac{\Delta\xi}{\Delta\chi}\left(\theta_{i+1,j}^{n} - \theta_{i,j}^{n}\right), \qquad (12\text{-}1)$$

$$\tilde{Q}_{\eta\,i,j}^{n+1} = (1-10\Delta\xi)\, Q_{\eta\,i,j}^{n} - \frac{\Delta\xi}{\Delta\eta}\left(\theta_{i,j+1}^{n} - \theta_{i,j}^{n}\right), \qquad (12\text{-}2)$$

$$\tilde{\theta}_{i,j}^{n+1} = \theta_{i,j}^{n} - \frac{\Delta\xi}{\Delta\chi}\left(Q_{\chi i+1,j}^{n} - Q_{\chi i,j}^{n}\right) - \frac{\Delta\xi}{\Delta\eta}\left(Q_{\eta i,j+1}^{n} - Q_{\eta i,j}^{n}\right), \qquad (12\text{-}3)$$

Corrector:

$$Q_{x\,i,j}^{n+1} = \frac{1}{2}\left[Q_{x\,i,j}^{n} + \tilde{Q}_{x\,i,j}^{n+1} - \frac{\Delta\xi}{\Delta\chi}\left(\tilde{\theta}_{i,j}^{n+1} - \tilde{\theta}_{i-1,j}^{n+1}\right) - 10\Delta\xi\, \tilde{Q}_{x\,i,j}^{n+1} \right], \qquad (12\text{-}4)$$

$$Q_{\eta\,i,j}^{n+1} = \frac{1}{2}\left[Q_{\eta\,i,j}^{n} + \tilde{Q}_{\eta\,i,j}^{n+1} - \frac{\Delta\xi}{\Delta\eta}\left(\tilde{\theta}_{i,j}^{n+1} - \tilde{\theta}_{i,j-1}^{n+1}\right) - 10\Delta\xi\, \tilde{Q}_{\eta\,i,j}^{n+1} \right], \qquad (12\text{-}5)$$

$$\theta_{i,j}^{n+1} = \frac{1}{2}[\theta_{i,j}^{n} + \tilde{\theta}_{i,j}^{n+1} - \frac{\Delta\xi}{\Delta\chi}(\tilde{Q}_{\chi\,i,j}^{n+1} - \tilde{Q}_{\chi\,i-1,j}^{n+1}) - \frac{\Delta\xi}{\Delta\eta}(\tilde{Q}_{\eta\,i,j}^{n+1} - \tilde{Q}_{\eta\,i,j-1}^{n+1})] \qquad (12\text{-}6)$$

To solve these finite difference equations, the same grid system as the radiative transfer problem is chosen. The non-dimensional time step for the thermal wave problem is selected as the same as the grid size, i.e., $\Delta\xi = \Delta\chi = \Delta\eta$, such that a unity Courant number is used.

RESULTS AND DISCUSSION

The sketch of the tissue geometry is shown in Fig. 1. For simplicity, we considered L = W = 15.395 mm such that $\chi_{\max} = \eta_{\max} = 1$ and the effect of tissue dimension on the temperature profile in the welding or soldering region is minimized. The width of the welding gap was 2.309 mm and the depth of the welding gap was W/5. The optical properties of the tissue were assume to be σ_a = 0. 1 mm^{-1} (selective absorption) and σ_s = 1.9 mm^{-1} (reduced scattering coefficient). We didn't consider the use of solder to enhance the absorption in the welding region. Thus, the optical properties in that region are assumed to be the same as the tissue. Other parameters include: α = 0.15 mm^2/s, $T_i = 310$ K, and $\rho C_p = 4.2\times10^6\ \mathrm{J/(m^3\cdot K)}$. The ultrashort laser pulse width was 10 ps and the width of incident laser sheet was 3.079 mm.

Figure 2 shows the profiles of the divergence of radiative heat flux along two straight lines in the optical axis direction at several selected time instants. For Fig. 2 (a) where $\eta = 0.5$ (it is the optical axis and center line), a steep gradient of the divergence of radiative heat flux is found for early time instant (t = 20 ps). As time advancing, the profiles become flat and the magnitude of overall strength decreases. At t = 200 ps, the profile shows a quite symmetric shape against the central point at $\chi = 0.5$ and its magnitude drops to the order of 10^{-11}. This implies that the radiation absorption of this pulse has almost been completed by this time stage. For Fig. 2 (b) where $\eta = 0.2$ (the line is away from the optical axis), the profile at t = 20 ps is even lower than that at t = 40 ps. This means that the peak laser intensity is delayed to reach the line. Generally the divergence of radiative heat flux is smaller than its counterpart in Fig. 2 (a). However, the difference between these two figures decreases as time matches. For example, the profiles in Figs. 2 (a) and (b) are quite similar at t = 100 ps and 200 ps, respectively.

Within the ultrashort time regime, the temporal profiles of temperatures at several selected positions are exhibited in Fig. 3. Two lateral positions ($\eta = 0.5$ and 0.4) and varying depth positions were chosen for comparison. At all locations, the temperature profiles increase rapidly within about 10 ps. Then they become very flat in a long time period. This is because radiation absorption can be completed in about one pulse width time duration. In most areas a stationary temperature profile is achieved within a time period of several pulse widths. Thus, we only need to compute the radiation heat transfer and initial local temperature response up to the order of 10 to 20 times of the laser pulse duration. In the following studies, the initial temperature field for heat conduction simulation are based on the local temperature profile obtained at time instant of t = 200 ps.

In Fig. 4, the spatial variance of temperature along the optical axis direction is investigated. The local temperature increases as time advances and then reaches to a pseudo stable condition at and after t = 200 ps but before thermal wave starts. It is seen that the gradient of the temperature variations along the optical axis (η = 0.5) is quite appreciable. However, the gradient for a position (η = 0.2) retarding from the optical axis is relatively smooth in the segment of χ < 0.2. It suggests that, it may be necessary to consider a non-direct irradiation to the welding area in order to improve the uniformity of heating.

Figure 5 shows the contours of the initial local temperature distribution at three time instants. At early time stage (t = 20 ps), the temperature field is concentrated on the laser deposition area but the magnitude of it is small. As time proceeds, the temperature field is propagating to the surrounding tissue due to radiation transport and the temperature reaches to a high level due to the accumulation of radiation absorption. After t = 100 ps and before the start of thermal wave propagation (may take t = 0.001τ), the local temperature field reaches to a steady state and maintained at a higher temperature value. If tissue closure would complete at this time period, it could minimize the thermal damage generated due to heat wave and diffusion.

Following the arrival of a pseudo stable local temperature field within a short time period the thermal wave propagation starts and the temperature field is governed by the hyperbolic

heat conduction equations. To validate the code for hyperbolic conduction simulation, a comparison between the present numerical simulation and a published analytical solution [26] for hyperbolic conduction in a 1-D slab is shown in Fig. 6. It is seen that the present calculations match the counterparts of analytical solution very well.

Now, the numerical simulation is extended to the 2-D welding case. The temperature profiles along three selected cross lines are exhibited in Figs. 7 (a), (b) and (c), respectively. Several time instants are selected for comparison. The wave behavior of temperature propagation is very obvious in the figures. The local temperature profiles at initial stage due to radiation absorption in the ultrashort time period show a perfect Gaussian distribution. Starting from $\xi = 0.05$ in Fig. 7 (a), the evolution of thermal waves takes place. The profiles are symmetric against the center. The amplitude of temperature wave gradually decreases as time marches. As the wave propagates from the center position to the tissue edge, the wave peak becomes small. At long time stage, the wave behavior retards and gradually disappears. Then the diffusion process starts. Similar wave behavior is shown in Fig. 7 (b) and (c) as well. However, the onset time of wave evolution is delayed to $\xi = 0.1$ in Fig. 7 (b) and to $\xi = 0.2$ in Fig. 7 (c). Interestingly, the hyperbolic temperatures in Fig. (c) are even higher than the local temperatures resulting from initial radiation absorption. This is the evidence of thermal wave propagation from the laser spotting area.

The hyperbolic temperature field in the tissue and its time histories are depicted in Fig. 8. At early time instants the temperature response is confined in a small area close to the laser spot. As time increases, the thermal influencing zone (higher temperature than surrounding area) enlarges with clear wave evolution inside the zone. At long time stage ($\xi = 0.5$), a diffusion field is forming in the whole tissue model.

To understand well the hyperbolic effects, the temperature profiles predicted by the hyperbolic model and Fourier parabolic model, respectively, are compared in Fig. 9, where the comparisons of the temporal variance of temperature profiles at different locations are presented. In hyperbolic conduction modeling, wave behavior exists and the temperature changes periodically with a decreasing amplitude. In parabolic conduction modeling, the temperature decays exponentially and more slowly than the hyperbolic prediction. Also the predicted maximum temperature values by the hyperbolic model are much larger than those by the parabolic model. In order to prevent the overheating in laser tissue welding, an appropriate hyperbolic model must be adopted for the heating time shortened than about five thermal relaxation times. Thereafter, a diffusion model is accurate as we can see from the comparisons in Fig. 9.

CONCLUSIONS

A mathematical model was developed to simulate the multi-scale and multi-physics heat transfer problem in ultrafast laser tissue welding and soldering. Subject to the incidence of an ultrashort laser pulse, the local temperature inside the tissue was found to rise very fast and this rise was purely because of local radiation absorption resulting from transient radiation heat transport. The radiation transport was more than 10 orders of magnitude faster than thermal wave propagation. During an ultrashort time period, the local temperature field reached to a pseudo steady state until the start of thermal wave propagation. The thermal wave phenomenon can be well described by the hyperbolic heat conduction equations. The wave behavior was observed from the contours of the 2-D temperature field as well as the temperature profiles along the optical axis and cross lines. The evolution of thermal wave took place earlier near the laser beam spot. As time increases, the thermal influencing zone enlarges with clear wave evolution inside the zone. The difference between hyperbolic modeling and parabolic modeling was obvious. In hyperbolic conduction modeling, wave behavior exists and the temperature changes periodically with a decreasing amplitude. In parabolic conduction modeling, however, the temperature decays exponentially and more slowly than the hyperbolic prediction. Also the predicted maximum temperature values by the hyperbolic model are much larger than those by the parabolic model. After about five thermal relaxation times, the difference between diffusion modeling and hyperbolic modeling is slight. In order to prevent the overheating in laser tissue welding and soldering, however, an appropriate hyperbolic model must be adopted since most reported tissue relaxation times are in the order of 10 sec in the literature.

ACKNOWLEDGMENTS

The authors acknowledge a subcontract from a NIH SBIR grant awarded to Creare Inc, NH. Z. Guo also acknowledges the partial support of this research from the New Jersey Space Grant Consortium (grant: NJSGC 03-44).

REFERENCES

1. T. Maiman, “Optical and microwave-optical experiments in ruby,” Phys. Rev. Lett., vol. 4, pp. 564-566, 1960.
2. L.S. Bass and M.R. Treat, “Laser tissue welding: A comprehensive review of current and future applications,” *Lasers Surg. Med*., vol. 17, pp.315-349, 1995.
3. N.M. Fried, V.C. Hung, and J.T. Walsh, “Laser tissue welding: Laser spot size and beam profile studies,” *IEEE J. Quantum Electronics*, vol. 5, pp.1004-1012, 1999.
4. D.P. Poppas, G.B. Rucker, and D.S. Scherr, “Laser tissue welding – poised for the new millenium,” *Surgical Technology International*, vol. IX, pp. 33-41, 2000.
5. K.M. McNally, B.S. Song, E.K. Chan, A.J. Welch, J. M. Dawes, and E. R. Owen, “Optimal parameters for laser tissue soldering. Part I: Tensile strength and scanning electron microscopy analysis,” *Lasers Surg. Med*., vol. 24, pp. 319-331, 1999.
6. L. W. Murray, L. Su, G.E. White, and R.A. White, “Cross linking of extracellular matrix proteins: A preliminary report on a possible mechanism of argon laser welding,” *Lasers Surg. Med*., vol. 9, pp.490-496, 1989.
7. R.P. Abergel, R. Lyons, R. Dwyer, R.A. White, and J. Uitto, “Use of lasers for closure or cutaneous wounds:

Experience with Nd:YAG, argon, CO_2 Lasers," *J. Dermatol Surg Oncol*, vol. 12, pp.1181-1185, 1986.
8. B.D. Byrd, D.L. Heintzelman, and K.M. McNally-Heintzelman, "Absorption properties of alternative chromophores for use in laser tissue soldering applications," *Biomed Sci Instrum*, vol. 39, pp. 6-11, 2003.
9. G.M. Leola, R.R. Anderson, S. Decocted, "Preliminary evaluation of collagen as a component in the thermally induced weld", *Proc SPIE*, vol. 1422, 116-122, 1991
10. L.L. Deckelbaum, J.M. Isner, R.F. Donaldson, S.M. Laliberte, R.H. Clarke, D.N. Salem, "Use of pulsed energy delivery to minimize tissue injury resulting from CO_2 laser irradiation of cardiovascular tissues", *J. Am Coll Cardiol*, vol. 7, pp. 898-900, 1986.
11. R.R. Anderson, and J.A. Parrish., "Selective photothermolysis: precise microsurgery by selective absorption of pulsed radiation", *Science*, vol. 220, pp. 525-527, 1983.
12. S. Kumar and K. Mitra, "Microscale aspects of thermal radiation transport and laser applications", in *Advances in Heat Transfer*, vol. 33, pp.187-294, 1998.
13. Z. Guo and S. Kumar, "Discrete ordinates solution of short pulse laser transport in two-dimensional turbid media", *Appl. Optics*, vol. 40, pp. 3156-3163, 2001.
14. Z. Guo and S. Kumar, "Three-dimensional discrete ordinates method in transient radiative transfer," *J. Thermophy. Heat Transfer*, vol. 16, pp. 289-296, 2002.
15. Z. Guo, J. Aber, B. Garetz and S. Kumar, "Monte Carlo simulation and experiments of pulsed radiative transfer," *J. Quantitative Spectroscopy & Rad. Transfer*, vol. 73, pp. 159 – 168, 2002.
16. Z. Guo and K.H. Kim, "Ultrafast-laser-radiation transfer in heterogeneous tissues with discrete-ordinates method", *Appl. Optics*, vol. 42, pp. 2897-2905, 2003.
17. K.H. Kim and Z. Guo, "Ultrafast radiation heat transfer in laser welding and soldeing", *Numerical Heat transfer Part A*, vol. 46, pp. 23-40, 2004.
18. A.J. Welch, E.H. Wissler and L.A. Priebe, "Significance of blood flow in calculation of temperature in laser irradiated tissue," *IEEE Trans. Biomed. Eng.*, vol. BME-27, pp. 164-166, 1980.
19. D.D. Joseph and L. Preziosi, "Heat waves", *Rev. Modern Phys.*, vol. 61, pp. 118-1128, 1989.
20. W. Kaminski, "Hyperbolic heat conduction equation for materials with a nonhomogeneous inner structures," *J. Heat Transfer*, vol. 112, pp. 555-560, 1990.
21. M.N. Ozisik and D.Y. Tzou, "On the wave theory in heat conduction," *J. Heat Transfer*, vol. 116, pp. 526-535, 1994.
22. Mitra K., Kumar S., Vedavarz A., and Moallemi M., 1995, "Experimental evidence of hyperbolic heat conduction in processed meat," *Trans of the ASME*, **117**, 568-573.
23. D. Y. Tzou, "Experimental support for the lagging behavior in heat propagation," *J. Thermophysics and heat transfer*, vol. 9, pp. 686-693, 1995.
24. A.S. Lavine and C. Bai, "Hyperbolic heat conduction in thin domains," *Thermal Sci. & Eng.*, vol. 2, pp. 185-190, 1994.
25. A. Vedavarz, S. Kumar and M.K. Moallemi, "Significance of non-Fourier heat waves in conduction," *J. Heat transfer*, vol. 116, pp. 221-224, 1994.
26. D.E. Glass, M.N. Ozisik, D.S. McRae, B. Vick, "On the numerical solution of hyperbolic heat conduction," *Numerical heat transfer*, vol. 8, pp. 497-504, 1985.
27. A. Saidane and S. H. Pulko, "High-power short pulse laser heating of low dimensional structures: a hyperbolic heat conduction study using TLM," *Microelectronic Engineering*, vol. 51-52, pp. 469-478, 2000.
28. L. H. Liu and H.P. Tan, "Non-Fourier effects on transient coupled radiative-conductive heat transfer in one-dimensional semitransparent medium subjected to a periodic irradiation," *J. Quantitative Spectroscopy & Rad. Transfer*, vol. 71, pp. 11-24, 2001.
29. Q.M, Fan and W.Q. Lu, "A new numerical method to simulate the non-Fourier heat conduction in a single-phase medium," *Int. J. Heat Mass Transfer*, vol. 45, pp. 2815-2821, 2002.
30. E. Hoashi, T. Yokomine, A. Shimizu and T. Kunugi, "Numerical analysis of wave-type heat transfer propagating in a thin foil irradiated by short-pulsed laser," *Int. J. Heat Mass Transfer*, vol. 46, pp. 4083-4095, 2003.
31. B. Choi and A.J. Welch, "Analysis of thermal relaxation during laser irradiation of tissue", *Lasers in Surg Med.*, vol. 29, pp. 351-359, 2001.
32. S.A. Telenkov, J.I. Youn, D.M. Goodman, A.J. Welch and T.E. Milner, "Non-contact measurement of thermal diffusivity in tissue," Phys. Med. Biol., vol. 46, pp. 551-558, 2001.

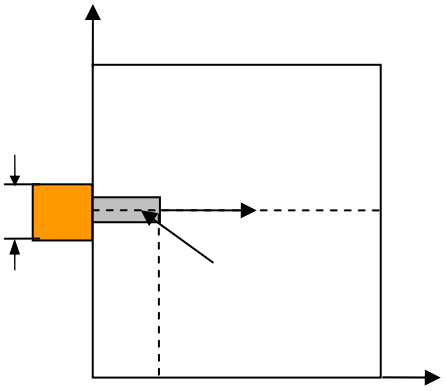

Fig.1. Schematic diagram of the simulation model.

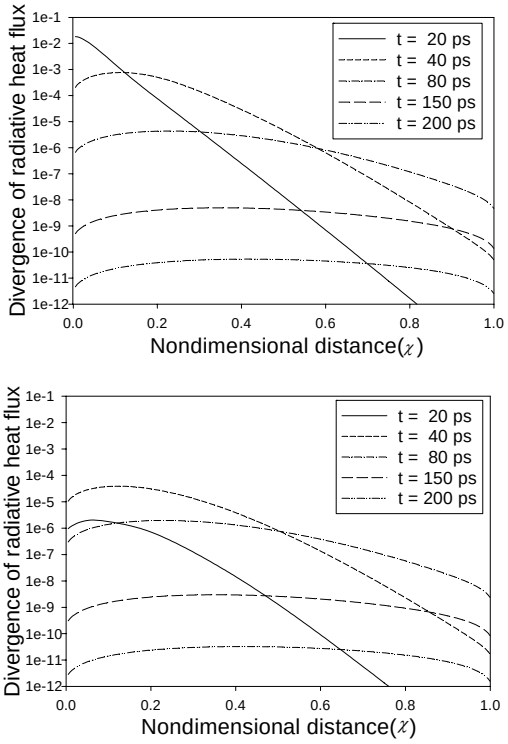

Fig. 2. The profiles of divergence of radiative heat flux along the optical axis direction with several selected time instants: (a) along the centerline of $\eta = 0.5$ and (b) along a line of $\eta = 0.2$.

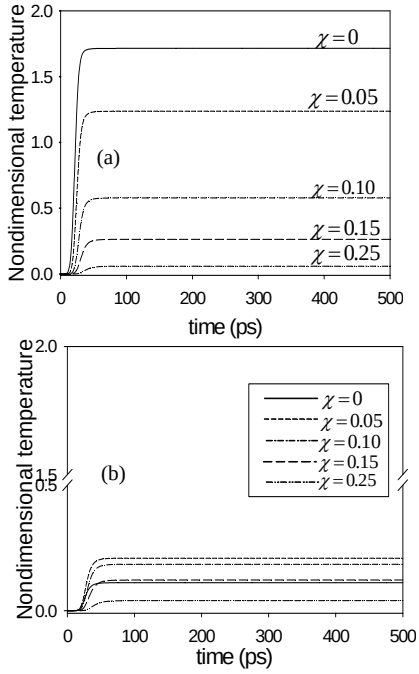

Fig. 3. The temporal profiles of initial temperature response at selected positions: (a) $\eta = 0.5$, and (b) $\eta = 0.4$

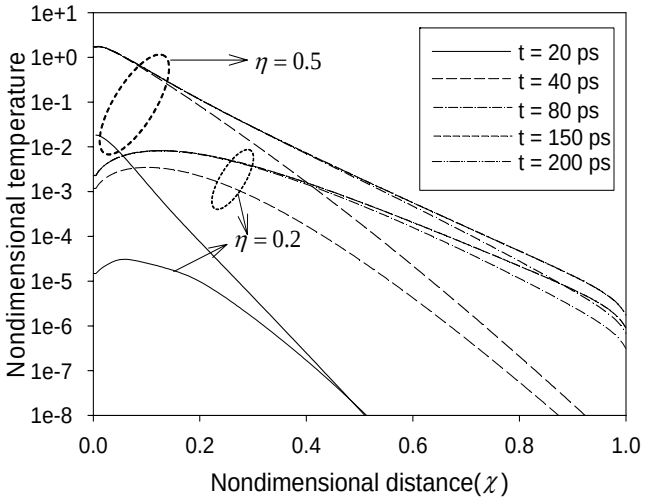

Fig. 4. The spatial variances of initial temperature along the optical axis direction for two different ordinate locations at several selected time instants.

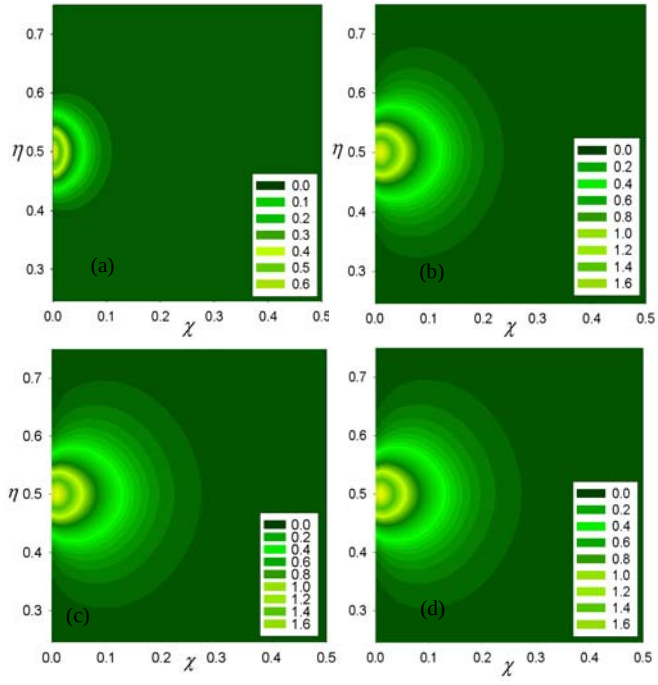

Fig. 5 The contours of initial temperature distribution at selected time instants at (a) t = 20 ps, (b) t = 40 ps, (c) t = 100 ps, and (d) t = 200ps.

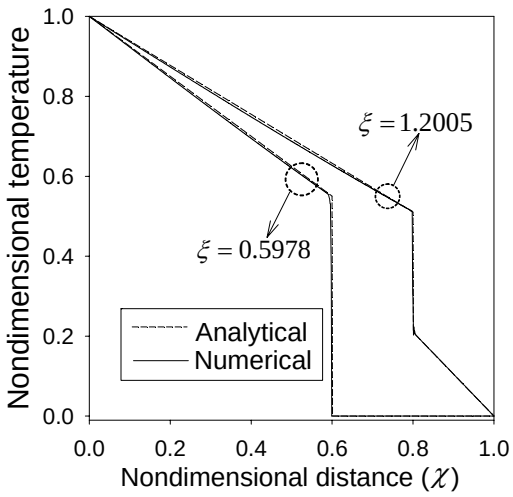

Fig. 6. Comparison between the numerical and exact solutions for an exemplary 1-D slab problem.

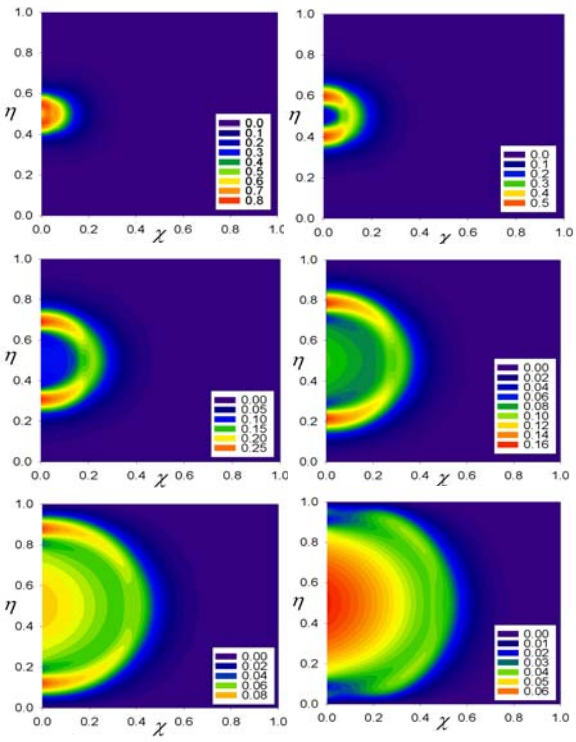

Fig. 7. The time histories of temperature profiles along three selected cross lines: (a) $\chi = 0$, (b) $\chi = 0.1$, and (c) $\chi = 0.2$.

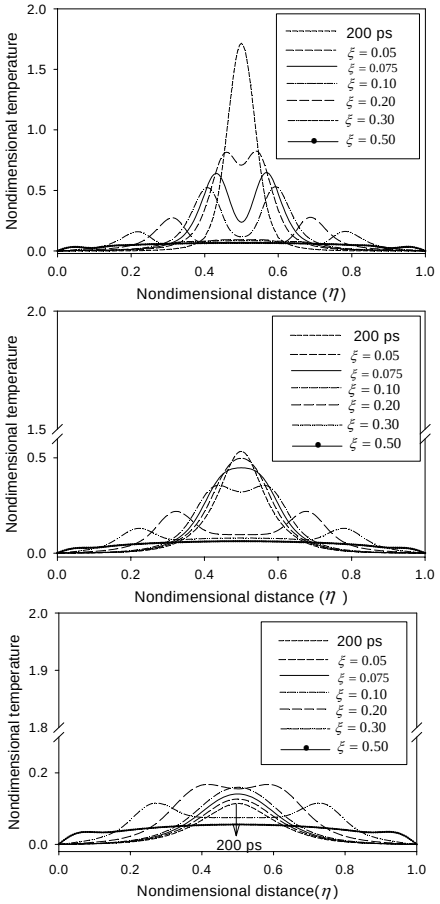

Fig. 8. The contours of hyperbolic conduction temperature field at several selected time instants: (a) $\xi = 0.05$, (b) $\xi = 0.1$, (c) $\xi = 0.2$, (d) $\xi = 0.3$,(e) $\xi = 0.4$,(f) $\xi = 0.5$

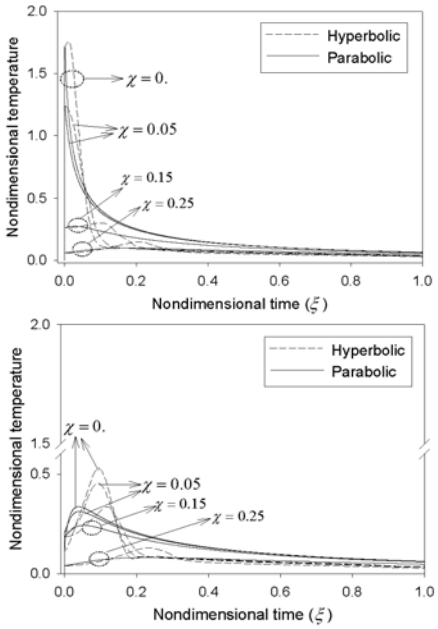

Fig. 9. Comparison of temporal profiles of temperature between hyperbolic conduction and parabolic conduction models: (a) $\eta = 0.5$, and (b) $\eta = 0.4$